JCTC Journal of Chemical Theory and Computation

Article

pubs.acs.org/JCTC

Free Energies from Dynamic Weighted Histogram Analysis Using Unbiased Markov State Model

Edina Rosta*,† and Gerhard Hummer‡

†Department of Chemistry, King's College London, London SE1 1DB, United Kingdom

‡Department of Theoretical Biophysics, Max Planck Institute of Biophysics, 60438 Frankfurt am Main, Germany

ABSTRACT: The weighted histogram analysis method (WHAM) is widely used to obtain accurate free energies from biased molecular simulations. However, WHAM free energies can exhibit significant errors if some of the biasing windows are not fully equilibrated. To account for the lack of full equilibration, we develop the dynamic histogram analysis method (DHAM). DHAM uses a global Markov state model to obtain the free energy along the reaction coordinate. A maximum likelihood estimate of the Markov transition matrix is constructed by joint unbiasing of the transition counts from multiple umbrella-sampling simulations along discretized reaction coordinates. The free energy profile is the stationary distribution of the resulting Markov matrix. For this matrix, we derive an explicit approximation that does not require the usual iterative solution of WHAM. We apply DHAM to model systems, a chemical reaction in water treated using quantum-mechanics/molecular-mechanics (QM/MM) simulations, and the Na^+ ion passage through the membrane-embedded ion channel GLIC. We find that DHAM gives accurate free energies even in cases where WHAM fails. In addition, DHAM provides kinetic information, which we here use to assess the extent of convergence in each of the simulation windows. DHAM may also prove useful in the construction of Markov state models from biased simulations in phase-space regions with otherwise low population.

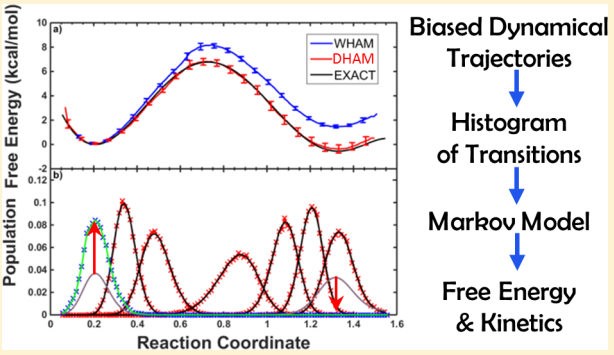

INTRODUCTION

Umbrella sampling (US)[1] is one of the most widely used methods for the calculation of accurate free energies from atomistic simulations. In US, multiple simulations are carried out with different biasing potentials to probe the probability distribution along a chosen reaction coordinate, which can be multidimensional. To combine the results of these different simulation windows into a global free energy profile, one typically employs the weighted histogram analysis method (WHAM),[2] as introduced by Ferrenberg and Swendsen,[3] building on ideas introduced by Bennett.[4,5] The key assumption underlying the WHAM analysis, even in its histogram-free formulations,[5−7] is that each simulation samples fully the corresponding equilibrium probabilities. This condition is often not fulfilled in practice.[8,9] Deviations from the equilibrium assumption occur if the runs in each window are too short, for example, as a result of slow dynamics in directions orthogonal to the chosen coordinates or because the umbrella windows are too wide and thus contain regions separated by barriers.

Here, we show that significant errors can be introduced in the WHAM-estimated free energy surfaces due to insufficient convergence in some of the US windows. To correct for this problem, we introduce a new dynamic histogram analysis method (DHAM) based on a transition probability matrix built from the simulation trajectories along the discretized reaction coordinates. DHAM is effectively a generalization of WHAM that uses transition probabilities in addition to histogram counts along the selected reaction coordinates. We show that WHAM is a special limiting case of DHAM. We also demonstrate that DHAM, as a maximum likelihood method, can achieve statistical accuracy comparable to WHAM when applied to the same data set. Additionally, because the local free energy profile is typically well converged, even when constructed from short simulations before overall equilibrium within a window is reached, DHAM significantly reduces the errors resulting from the WHAM analysis of poorly converged simulations.

When using WHAM, it is assumed that the biased simulations are long enough, such that equilibrium is reached in each simulation window over the full range of the reaction coordinates employed. Whereas correction factors have been introduced for correlations between sequential histogram counts,[3] the lack of full convergence to equilibrium in a window is not accounted for. However, in actual simulations, complete equilibration in all windows is practically never achieved, which can lead to significant errors when applying WHAM. The significant error made in case of insurmountable barriers can be illustrated in a two-configuration model, where at equilibrium the system has equal probabilities of 1/2 to be at

Received: August 7, 2014

DOI: 10.1021/ct500719p
J. Chem. Theory Comput. XXXX, XXX, XXX−XXX

positions x_1 and x_2, and zero probability to be anywhere else. We now consider an umbrella sampling simulation with two windows run for N_1 and N_2 steps, centered at x_1 and x_2, using a harmonic bias with force constants K_1 and K_2, respectively, for each window. In this case, there is no overlap between the two simulations. Nevertheless, WHAM provides an estimate for the free energy difference between the two states (see Appendix A for details):

$$\frac{p_2}{p_1} = e^{-\Delta G/k_B T} \approx \sqrt{\frac{N_2}{N_1}}\, e^{-(x_2-x_1)^2(K_2-K_1)/4k_B T} \tag{1}$$

$$\Delta G \approx (x_2 - x_1)^2(K_2 - K_1)/4 + k_B T/2 \ln \frac{N_1}{N_2} \tag{2}$$

p_1 and p_2 are the equilibrium populations in basins 1 and 2, respectively, as estimated from WHAM, k_B is the Boltzmann constant, and T the absolute temperature. The corresponding estimate ΔG of the free energy difference is entirely artificial, since no equilibrium has been achieved due to the insurmountable barrier. This issue is particularly relevant in the analysis of simulation trajectories generated with weak biasing potentials. In this case, regions within a simulation window may be separated by significant barriers even on the biased free energy surface, preventing full equilibration in the respective windows. Analyzed under the violated assumption of local equilibrium, such windows can influence the overall free energy profile in an artificial way, causing significant errors.

Here, we propose the DHAM analysis algorithm to alleviate this problem by explicitly accounting for the time dependence in molecular simulations (where "time" would be the number of steps in a Monte Carlo simulation). In effect, we deduce a common underlying Markov state model together with the global free energy profile from multiple simulations that may be short and may have different biasing potentials. Note that our approach differs from MSM approaches used in molecular simulations[10−13] in that we define Markov states based on discretized reaction coordinates rather than using coarse-grained states. In the original WHAM formulation, correlations between the data were accounted for using a simple dynamic relaxation model.[3] Here, we go beyond and assume that the trajectories capture the local transition probabilities for motion along the reaction coordinate on the sampling time scale and that these transitions are Markovian. Our approach is related to earlier work that exploited the fact that the equilibrium distribution is stationary under time-propagation, with transition counts extracted from short-time trajectories,[14] as formalized by Adib using microscopic time-reversibility.[15] To estimate the free energies from short runs, we use a maximum likelihood approach, as was done, for example, by Sriraman et al.[16] via the stationary distribution of a master equation satisfying detailed balance that is determined from short (or long) trajectories, Sakuraba et al.,[9] or Wu and Noé,[8] who developed a procedure without explicit assumption of a dynamical model. More recently, Mey, Wu, and Noe developed other (nonmaxmimum likelihood) estimators of the free energy that combine information from different states.[17] Building on the general theory, we derive an explicit estimate for the unbiased Markov transition matrix using an unbiasing strategy that is exact in the limit of diffusive dynamics with short time t.[18] We note that this Markov matrix contains both energetic and dynamic information for the motion along the reaction coordinate. It can thus also be used to model the projected dynamics along the chosen reaction coordinate and, in particular, to estimate barrier-crossing rates in addition to the underlying free energy profile.

In the following, we first introduce the general theory. We then derive an explicit expression for the Markov matrix of transition probabilities for the original system without biasing potentials. Using this expression, we study a number of illustrative applications, from simple model systems to the calculation of a chemical reaction barrier in solution and of the free energy surface for ion conduction through a membrane-embedded ion channel. After discussing implications, applications, and possible problems, we work out the full nonlinear maximum-likelihood problem of constructing a Markov transition matrix in Appendix B.

THEORY

Our goal is to find the equilibrium free energy along the chosen reaction coordinate x in a way that takes into account dynamical information, that is, information about time propagation and the resulting time correlations. We start by dividing x into small bins. Note that the coordinate can be multidimensional, with i then indexing the multidimensional bins. The free energy G_i is related to the normalized equilibrium probabilities of bin i through $G_i = -k_B T \ln p_i$, with k_B the Boltzmann constant and T the absolute temperature. In the following, we will analyze trajectory data with a maximum-likelihood method to construct a Markov transition matrix that has p_i as its stationary distribution. For comparison, the traditional WHAM estimate for p_i is obtained as the maximum-likelihood solution under the assumption that all trajectory points are independent and drawn from the respective equilibrium distribution in each window.[19] In this limit, as shown below, the estimates of WHAM and DHAM indeed are consistent.

Likelihood Function. By projecting the trajectories of the different US biasing windows into bins along the reaction coordinates, we obtain discrete time series of the bin indices, assuming for simplicity that the time steps Δt are uniform and equal in all US simulations. From these data, we build the transition-count matrices $T^{(k)}$ for each simulation k. These simulations are typically run on different potential surfaces, with added bias potentials $u^{(k)}(x)$ but may also be on identical surfaces or even without bias. An element of the matrix, $T_{ji}^{(k)}$ denotes the integer number of the observed transitions from bin i to bin j in simulation k. Under the Markov assumption of uncorrelated transitions, the likelihood of observing a given number of transitions in simulation k is proportional to the following product,

$$\Pr^{(k)} \propto \prod_{i=1}^{N_{bin}} \prod_{j=1}^{N_{bin}} (M_{ji}^{(k)})^{T_{ji}^{(k)}} \tag{3}$$

where $M_{ji}^{(k)}$ is the Markov transition probability (or Green's function or propagator at the fixed lag time) of simulation k, defined as the probability that a trajectory originally in bin i is in bin j at a time interval Δt later. The log likelihood function over all simulations is given as

$$\tilde{L} = \ln \prod_{k=1}^{N_{Sim}} \prod_{i=1}^{N_{bin}} \prod_{j=1}^{N_{bin}} (M_{ji}^{(k)})^{T_{ji}^{(k)}} = \sum_{k=1}^{N_{Sim}} \sum_{i=1}^{N_{bin}} \sum_{j=1}^{N_{bin}} T_{ji}^{(k)} \ln M_{ji}^{(k)} \tag{4}$$

DOI: 10.1021/ct500719p
J. Chem. Theory Comput. XXXX, XXX, XXX−XXX

To relate the biased transition probability matrices, $M_{ji}^{(k)}$ to the underlying unbiased transition probability matrix, M_{ji}, we introduce without loss of generality a coefficient matrix $c_{ji}^{(k)}$ in the following column-normalized form using the normalization factors $f_i^{(k)}$:

$$M_{ji}^{(k)} = f_i^{(k)} c_{ji}^{(k)} M_{ji} \tag{5}$$

To ensure that the outgoing transition probabilities of the unbiased and biased transition matrices are normalized to 1, we add Lagrange multipliers to the log likelihood function:

$$L = \ln \prod_{k=1}^{N_{\mathrm{Sim}}} \prod_{i=1}^{N_{\mathrm{bin}}} \prod_{j=1}^{N_{\mathrm{bin}}} (M_{ji}^{(k)})^{T_{ji}^{(k)}} + \sum_{k=1}^{N_{\mathrm{Sim}}} \sum_{i=1}^{N_{\mathrm{bin}}} \lambda_i^{(k)} (1 - \sum_{j=1}^{N_{\mathrm{bin}}} M_{ji}^{(k)}) + \sum_{i=1}^{N_{\mathrm{bin}}} \mu_i (1 - \sum_{j=1}^{N_{\mathrm{bin}}} M_{ji}) \tag{6}$$

Substituting eq 5, we obtain

$$L = \sum_{k=1}^{N_{\mathrm{Sim}}} \sum_{i=1}^{N_{\mathrm{bin}}} \sum_{j=1}^{N_{\mathrm{bin}}} T_{ji}^{(k)} \ln(f_i^{(k)} c_{ji}^{(k)} M_{ji}) + \sum_{k=1}^{N_{\mathrm{Sim}}} \sum_{i=1}^{N_{\mathrm{bin}}} \lambda_i^{(k)} (1 - \sum_{j=1}^{N_{\mathrm{bin}}} f_i^{(k)} c_{ji}^{(k)} M_{ji}) + \sum_{i=1}^{N_{\mathrm{bin}}} \mu_i (1 - \sum_{j=1}^{N_{\mathrm{bin}}} M_{ji}) \tag{7}$$

We find the maximum of L by taking the derivatives with respect to the parameters and setting them to zero. For $f_i^{(k)}$ we find

$$\frac{\partial L}{\partial f_i^{(k)}} = \sum_{j=1}^{N_{\mathrm{bin}}} \frac{T_{ji}^{(k)}}{f_i^{(k)}} - \sum_{j=1}^{N_{\mathrm{bin}}} \lambda_i^{(k)} c_{ji}^{(k)} M_{ji} = 0 \tag{8}$$

This relation allows us to express the Lagrange multipliers $\lambda_i^{(k)}$ in terms of the count matrix,

$$\lambda_i^{(k)} = \frac{\sum_{j=1}^{N_{\mathrm{bin}}} T_{ji}^{(k)}}{\sum_{j=1}^{N_{\mathrm{bin}}} c_{ji}^{(k)} M_{ji} f_i^{(k)}} = \sum_{j=1}^{N_{\mathrm{bin}}} T_{ji}^{(k)} = n_i^{(k)} \tag{9}$$

where we used the normalization condition and introduced $n_i^{(k)}$ as the number of transitions that were initiated in bin i of simulation k. By setting the derivative of L with respect to $\lambda_i^{(k)}$ to zero, we obtain an expression for $f_i^{(k)}$:

$$f_i^{(k)} = (\sum_{j=1}^{N_{\mathrm{bin}}} c_{ji}^{(k)} M_{ji})^{-1} \tag{10}$$

By maximizing L with respect to M_{ji}, we obtain

$$\frac{\partial L}{\partial M_{ji}} = \sum_{k=1}^{M_{\mathrm{sim}}} \frac{T_{ji}^{(k)}}{M_{ji}} - \sum_{k=1}^{M_{\mathrm{sim}}} \lambda_i^{(k)} f_i^{(k)} c_{ji}^{(k)} - \mu_i = 0 \tag{11}$$

Combining eqs 9 and 11, we obtain the following expression for M_{ji}:

$$M_{ji} = \frac{\sum_{k=1}^{M_{\mathrm{sim}}} T_{ji}^{(k)}}{\mu_i + \sum_{k=1}^{M_{\mathrm{sim}}} n_i^{(k)} f_i^{(k)} c_{ji}^{(k)}} \tag{12}$$

This expression will form the basis for the DHAM method.

Effect of Biasing Potentials. In US, the unbiased potential surface is modified by applying a (typically harmonic) bias potential $u_i^{(k)}$ in each window k. This bias is evaluated at the center of the ith bin in the kth simulation, which for a harmonic potential centered at $x^{(k)}$ would result in

$$u_i^{(k)} = \frac{1}{2} K^{(k)} (x_i - x^{(k)})^2 \tag{13}$$

where $K^{(k)}$ is the force constant.

In the following, we construct a family of coefficient matrices $c_{ji}^{(k)}$ that capture both the limits of diffusion along the reaction coordinate at short time steps Δt and of uncorrelated sampling of the equilibrium distribution at long time steps. For diffusive dynamics at short time steps, the presence of a biasing potential changes the transition probability to

$$M_{ji}^{(k)} \propto M_{ji} \exp[-(u_j^{(k)} - u_i^{(k)})/2k_{\mathrm{B}}T] \tag{14}$$

which follows, for example, from a spatial discretization of the Smoluchowski diffusion equation.[18] Note that in the limit of short times, M_{ji} will be diagonally dominated. By contrast, at long time steps Δt the transitions are independent of the starting index i,

$$M_{ji} \propto p_j \quad \text{and} \quad M_{ji}^{(k)} \propto \exp(-u_j^{(k)}/k_{\mathrm{B}}T) p_j \tag{15}$$

and M_{ji} will be dense.

For the coefficient matrix

$$c_{ji}^{(k)} = \exp[-(w u_j^{(k)} - (1 - w) u_i^{(k)})/k_{\mathrm{B}}T] \tag{16}$$

the two extremes of short and long time steps are exactly recovered for $w = {}^1/_2$ and $w = 1$, respectively. This functional form will be used in the following. In this approximation, we thus express the effect of adding a bias potential $u^{(k)}$ in simulation k as a product of the matrix M_{ji} common to all windows and a correction term that depends only on the biasing potential. More involved approaches are of course possible. For instance, one could simultaneously estimate a position-dependent diffusion coefficient and a free energy surface.[20] However, such approaches require more involved numerical analysis.

Approximate Explicit Solution. By invoking the detailed balance condition, we derive in the following an explicit expression for the transition matrix. In this way, we avoid the need for finding solutions to coupled nonlinear equations resulting from full likelihood maximization (see Appendix B). As a consequence of detailed balance, $M_{ji}p_i = M_{ij}p_j$ and $M_{ji}^{(k)}p_i^{(k)} = M_{ij}^{(k)}p_j^{(k)}$, the equilibrium probabilities $p_i^{(k)}$ in bin i of window k satisfy:

$$\frac{M_{ji}^{(k)}}{M_{ij}^{(k)}} \frac{p_i^{(k)}}{p_j^{(k)}} = \frac{f_i^{(k)} c_{ji}^{(k)} M_{ji}}{f_j^{(k)} c_{ij}^{(k)} M_{ij}} \frac{p_i}{p_j} \frac{\exp(-u_i^{(k)}/k_{\mathrm{B}}T)}{\exp(-u_j^{(k)}/k_{\mathrm{B}}T)} = 1 \tag{17}$$

rewritten in terms of the unbiased transition matrix M_{ji} and the bias energies $u_i^{(k)}$. Since the exact transition matrix should also satisfy detailed balance, we obtain

$$\frac{f_i^{(k)} c_{ji}^{(k)}}{f_j^{(k)} c_{ij}^{(k)}} = \frac{\exp(-u_j^{(k)}/k_{\mathrm{B}}T)}{\exp(-u_i^{(k)}/k_{\mathrm{B}}T)} \tag{18}$$

Note, however, that the numerical estimate of M_{ji} may violate detailed balance, as discussed in Appendix B.

DOI: 10.1021/ct500719p
J. Chem. Theory Comput. XXXX, XXX, XXX−XXX

This relation is satisfied exactly by $f_i^{(k)} c_{ji}^{(k)} = \exp[-(w u_i^{(k)} - (1 - w) u_i^{(k)})/k_B T]$. With this approximation, we arrive at an explicit expression for the elements of the Markov transition matrix:

$$M_{ji} = \frac{\sum_{k=1}^{M_{sim}} T_{ji}^{(k)}}{\mu_i + \sum_{k=1}^{M_{sim}} n_i^{(k)} \exp(-(w u_j^{(k)} - (1 - w) u_i^{(k)})/k_B T)} \tag{19}$$

where the Lagrange multipliers μ_i can be calculated by solving the following equations

$$\sum_{j=1}^{N_{bin}} M_{ji} = 1 = \sum_{j=1}^{N_{bin}} \frac{\sum_{k=1}^{M_{sim}} T_{ji}^{(k)}}{\mu_i + \sum_{k=1}^{M_{sim}} n_i^{(k)} \exp(-(w u_j^{(k)} - (1 - w) u_i^{(k)})/k_B T)} \tag{20}$$

which can be cast into a polynomial form of order N_{bin}. As an explicit approximation that does not require the numerical solution of these equations, we can obtain a normalized transition matrix simply by normalizing the columns:

$$M_{ji} = \frac{M_{ji}^{unnorm}}{\sum_{l=1}^{N_{bin}} M_{li}^{unnorm}} \tag{21}$$

where M_{ji}^{unnorm} is obtained by setting $\mu_i = 0$ in eq 19. In our practical applications, we concentrate on the short-time approximation for $w = {}^1/_2$:

$$M_{ji}^{unnorm} = \frac{\sum_{k=1}^{M_{sim}} T_{ji}^{(k)}}{\sum_{k=1}^{M_{sim}} n_i^{(k)} \exp(-(u_j^{(k)} - u_i^{(k)})/2k_B T)} \tag{22}$$

which is then column normalized. The equilibrium probabilities p_i can be calculated as the eigenvector corresponding to eigenvalue 1 of the transition matrix M_{ji}, that is, as its invariant distribution. This eigenvector can be obtained also directly as the normalized nontrivial solution of the following system of linear equations,

$$\sum_{j=1}^{Nbin} M_{ij} p_j = p_i \tag{23}$$

These equations can be solved, for example, by setting any (nonzero) p_j to 1 initially, solving the resulting $N_{bin} - 1$ linear equations, and then normalizing the resulting p_i values. Importantly, when the barriers separating the metastable states are high, then the eigenvalue 1 will be nearly degenerate. In this case, high numerical accuracy is required.

Recovering WHAM. In the limit of uncorrelated trajectory data, we recover the WHAM equations. In WHAM, no time information is used, and perfect equilibrium sampling is assumed. In our theoretical framework, this corresponds to a complete loss of memory of the bin from which a transition started. In this limit, the transition probability M_{ji} becomes the equilibrium probability P_j of j, independent of i. Starting bins no longer enter, and can thus be lumped together into a single "bin" I. We then arrive at

$$p_j = M_{jI} = \frac{\sum_{k=1}^{M_{sim}} T_{jI}^{(k)}}{\sum_{k=1}^{M_{sim}} n_I^{(k)} f_I^{(k)} c_{jI}^{(k)}} \tag{24}$$

In this limit, the counts $T_{jI}^{(k)}$ are the histogram counts of observing a data point in bin j, and the total counts $n_I^{(k)}$ are the number of data points in the simulation, $N^{(k)}$:

$$p_j = \frac{\sum_{k=1}^{M_{sim}} n_j^{(k)}}{\sum_{k=1}^{M_{sim}} n_I^{(k)} f_I^{(k)} c_{jI}^{(k)}} \tag{25}$$

For simulations that are long enough compared to their equilibration times, the $c_{jI}^{(k)}$ approach $\exp(-u_j^{(k)})$, $w = 1$ and reflecting the proper equilibrium probabilities using the bias $u^{(k)}$, and also satisfying detailed balance (see eq 18). This gives us the well-known WHAM equations, with the normalization constant $f^{(k)}$ (where we drop the index I):

$$p_j = \frac{\sum_{k=1}^{M_{sim}} n_j^{(k)}}{\sum_{k=1}^{M_{sim}} N^{(k)} f^{(k)} \exp(-u_j^{(k)}/k_B T)} \tag{26}$$

and

$$f^{(k)} = \frac{1}{\sum_{l=1}^{N_{bin}} \exp(-u_l^{(k)}/k_B T) p_l} \tag{27}$$

We note that the two different implementations of WHAM—with or without binning—differ by how the normalization constants ($f^{(k)}$) are determined. The MBAR version without binning[5] is equivalent to the regular binned version of WHAM in the limit of infinitesimally small bin sizes.[21] In practice, the numerical results for "WHAM" presented in this paper are based on a binless form,[21] but the different implementations provide essentially identical results.

Formally, DHAM and WHAM are therefore closely related in the limit of uncorrelated data. However, simply setting $w = 1$ does not produce the WHAM result, even after full likelihood optimization as described in Appendix B. The reason is that the chosen functional form of $c_{ji}^{(k)}$ does not enforce the limit of M_{ji} going to p_j, as w approaches 1.

Relaxation Time. For each window k, we can estimate the relaxation time from the second-largest eigenvalue $\lambda_2^{(k)}$, with $\lambda_1^{(k)} = 1$. These eigenvalues can be calculated for the model transition matrix of window k, $M_{ji}^{(k)} = f_i^{(k)} c_{ji}^{(k)} M_{ji}$. In this way, separated regions that may not have been sampled are also taken into account. By contrast, the actual time series in simulation k alone may not be fully converged. The DHAM estimate of the characteristic relaxation time is then

$$\tau^{(k)} = -1/\ln \lambda_2^{(k)} \tag{28}$$

in units of the lag time between transitions. Ideally, the simulation time T_k in window k should exceed this relaxation time:

$$T_k \gg \tau^{(k)} \tag{29}$$

Unbiased Simulations. For unbiased simulations our formulas are exact if the Markov assumption is valid, and the overall formula reduces to a simple ratio of averages.[8]

$$M_{ji} = \frac{\sum_{k=1}^{M_{sim}} T_{ji}^{(k)}}{\sum_{k=1}^{M_{sim}} n_i^{(k)}} \tag{30}$$

Kinetics from DHAM. The matrix M_{ji} defines a Markov state model for motions between the bins and thus also contains relevant kinetic information. This kinetic information can be extracted in a variety of ways, for example, by determining the global relaxation times and correlation function using a spectral expansion,[22] or by estimating local diffusion coefficients.[20] At least at an approximate level, one can thus

DOI: 10.1021/ct500719p
J. Chem. Theory Comput. XXXX, XXX, XXX−XXX

estimate barrier-crossing times directly from the global DHAM analysis of local US trajectories.

RESULTS

1D Model Potential. To illustrate possible significant errors introduced by WHAM when using weak or no bias, we studied an asymmetrical double well model system (Figure 1).

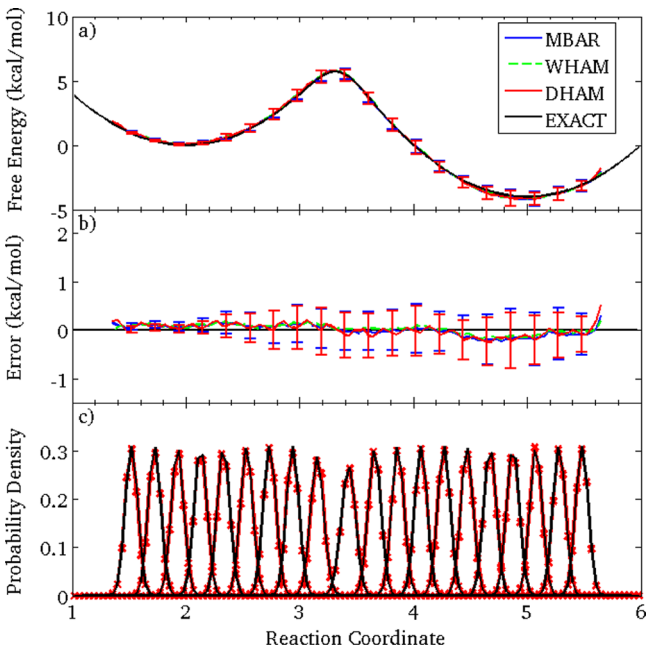

Figure 1. (A) Free energy profile using umbrella sampling simulations on a model potential (black line). The free energy is reconstructed from 20 parallel umbrella sampling simulations 3000 Monte Carlo steps each, with 200 kcal/mol biasing spring constants, see text) using WHAM (blue line with error bars) and our method (red line with error bars). (B) The mean error with respect to the underlying model potential. (C) The probability densities of the 20 umbrella windows. The equilibrium population is calculated as the average population in each window over the 5 independent US simulations with the harmonic biasing constraint added to the underlying model potential as described above (red line and symbols). The corresponding exact underlying equilibrium population is also shown (black line).

The 1D free energy surface, $G(x)$ along x, is defined as the following function:

$$G(x) = -2\ln[e^{-2(x-2)^2-2} + e^{-2(x-5)^2}] + c$$

$G(x)$ is given in kcal/mol, with k_BT = 0.596 kcal/mol. The constant c is chosen to give a potential of 0 kcal/mol at the minimum of the reactant state. First, we modeled standard US simulations on this surface by carrying out Monte Carlo (MC) simulations using 20 uniformly distributed umbrella windows in the range [−1.5, 5.5], with K = 200 kcal/mol biasing spring constants. 3000 Monte Carlo steps were run in each window using a random displacement from a uniform distribution in [−0.1, 0.1]. Both WHAM and DHAM reconstruct the original free energy profile successfully (Figure 1). Error bars were obtained by running 5 independent sets of US simulations. Importantly, both methods show the same magnitude for the statistical error.

Second, we tested the effects of weak biasing potentials, which may result in significant errors in the free energy calculated from WHAM because the assumption of equilibrium in each window is violated. This effect is illustrated by changing the spring constant of the biasing potentials in the first three umbrella windows (centered at 0.50, 1.71, and 1.92, respectively) of the previous example to 1 kcal/mol (Figure 2), leaving all other simulation parameters identical. Since these

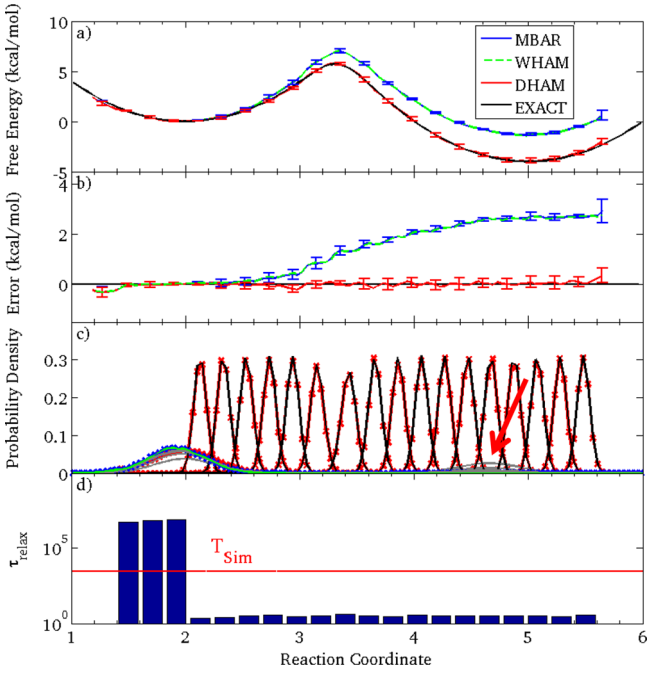

Figure 2. (A) Free energy profile using umbrella sampling simulations on a model potential (black line). The free energy is reconstructed from 20 parallel umbrella sampling simulations using WHAM/MBAR (blue/green line with error bars) and our method (red line with error bars). The first three of the 20 windows has a smaller, 1 kcal/mol biasing force. (B) The mean error with respect to the underlying model potential. (C) Equilibrium populations are only locally but not globally correct in the simulations of the first three umbrella windows. The equilibrium population is calculated as the average population over 5 independent MC simulations (3000 steps each) with a harmonic biasing constraint added to the underlying model potential as described above (red line and symbols). The corresponding exact underlying equilibrium population is also shown (black line). To highlight the first umbrella window, populations are shown in blue (line and symbol). The population corresponding to the exact underlying biased potential normalized to the first half of the full reaction profile (green line) is also shown to permit a better comparison with the simulation data in this umbrella window (blue line and symbols). The red arrow points to the significant tail corresponding to the exact populations of the first three umbrella windows (gray lines). (D) Relaxation times calculated according to eq 28 within the 20 umbrella windows as a function of the constraint position (blue bars, log scale). For comparison, the duration T_{sim} of the simulations in each window is also shown (red line, log scale).

windows are positioned in the reactant valley, overall the entire x-range is still well sampled. However, the underlying assumption of WHAM that each umbrella window samples the corresponding free energy profile is no longer satisfied. The simulation data in the first three windows, although locally sampling the equilibrium probability accurately, fail to sample a second population in the product valley (Figure 2), which is also significant due to the small biasing constraint. This situation is not improved with any reasonable extension of the simulation length due to the large barrier between the two states in the biased simulations. Despite the fact that the

DOI: 10.1021/ct500719p
J. Chem. Theory Comput. XXXX, XXX, XXX−XXX

product state umbrella windows are disconnected from the reactant state, the WHAM analysis of the data nevertheless combines these two windows using the underlying assumption of global convergence, and provides a prediction for the free energy difference analogously to what is shown in eq 2, thus leading to a significant overestimation of the product free energies. As a practical protocol, narrower umbrella windows with larger biasing force constants could thus be numerically more robust in US simulations when using WHAM for analysis.

To assess the predicted equilibration time in each window, we calculated the relaxation times of each biased simulation in the 20 windows according to eq 28 (Figure 2D). The windows with smaller bias have orders of magnitude larger relaxation times than the total simulation times and than the relaxation times of the windows with large biasing forces. In such "non-equilibrium" simulations DHAM should be used instead of WHAM. We note that related convergence errors can also be detected by the analysis of Zhu and Hummer,[23] in particular the relative-entropy consistency check using the Kullback–Leibler distance (eq 41 in ref 23) between the local and global distributions. This analysis indeed predicts about an order of magnitude larger η values for the first three simulation windows as compared to the other windows (data not shown). As DHAM only relies on locally converged sampling of the free energy profile, it correctly reproduces the free energy profile even with weak biasing potentials and thus can be used even in situations where full equilibration is not achieved.

The example corresponding to Figure 2 can be further extrapolated to simulations with no applied bias. Free downhill simulations can also be analyzed using DHAM, which reduces to the even simpler form of eq 30 in this case. Analogous methods have been used to reconstruct free energy profiles of nonequilibrium relaxation trajectories.[14,20,24] In our case, there is no need to fit a nonuniform diffusion constant along the reaction coordinate, since variations are already accounted for in the Markov state formalism. To illustrate this, we run 100 downhill MC trajectories (5000 steps each) that were initiated near the transition state region at x = 3.4. The free energy can be accurately reconstructed (Figure 3) despite the significant barrier height. Note that denser binning was required for the discretization of the reaction coordinate, and also significantly more simulation data were needed for the convergence of the free energy profile than in the US simulations above. WHAM, however, cannot be used to provide the correct free energy estimate for this nonequilibrium simulation data, as it incorrectly predicts a local minimum for the barrier region where the simulation trajectories were repeatedly initiated.

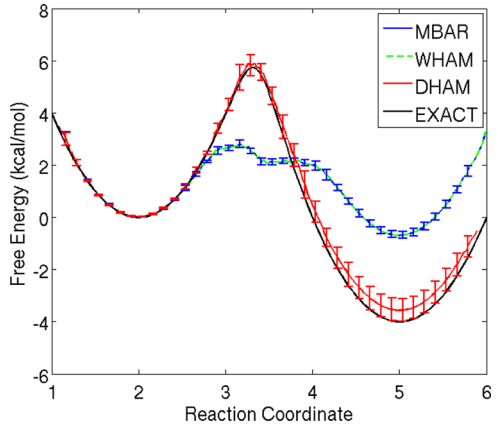

Figure 3. Free downhill simulations from near the top of the barrier on a model potential (black line). The free energy is reconstructed from 100 downhill trajectories (5000 Monte Carlo steps each, without any biasing force added, starting each trajectory from the reaction coordinate x = 3.4) using WHAM (blue line with error bars) and our method (red line with error bars). The error bars are obtained from 5 simulation sets with the same parameters.

2D Model Potential. Poorly chosen reaction coordinates with missing important degrees of freedom pose common problems in free energy calculations of complex processes. We present here a 2D model potential where the 1D-projected free energy profile significantly underestimates the free energy barrier (Figure 4).[25] The 2D model potential is constructed using the following underlying analytical free energy function:

$$G(x,y) = -\ln[e^{-\gamma((x+2)^2+(y+2)^2)} + e^{-\gamma((x-2)^2+(y-1)^2)} + e^{-\gamma((x+3)^2+5y^2+2)} + e^{-\gamma((x-3)^2+5(y+1)^2-2)}] + c$$

$G(x,y)$ is given in kcal/mol with k_BT = 0.596 kcal/mol, γ = 100.0, and c is chosen such that $G(x,y)$ is zero at the global minimum.

We first examined whether DHAM can recover the 2D free energy profile (Figure 4). We carried out US simulations with harmonic constraints centered on a 16 by 16 grid in each dimension, spanning the reaction coordinate values from −2.8 to 2.8, symmetrically both for x and y coordinates. The biasing forces of 40 kcal/mol were used uniformly. The obtained unbiased 2D profile (Figure 4B) accurately reproduces the exact potential.

Next, we tested the projection of the free energy profile to coordinate x only. This profile is recovered by projecting the full 2D DHAM free energy surface on the 1D (x) reaction coordinate (Figure 5, blue line obtained with DHAM, black line is the exact result). However, even the exact projected 1D profile has a barrier of less than 2 kcal/mol and thus does not capture the main ∼5.5 kcal/mol barrier for the full 2D system. As a result, the 1D profile cannot correctly account for the dynamics of the system. Indeed, the Markov model and the corresponding free energies obtained along x are inconsistent with the one obtained from the projection of the full 2D profile (Figure 4) or by regular WHAM. Therefore, large discrepancies between DHAM and WHAM estimates of the free energy signal that important reaction coordinates may be missing. Such problems might then be addressed by probing different coordinates, extending the dimensionality of the DHAM models, or by using a hidden Markov model formalism. Exploring the use of these more complex dynamic models in free energy calculations will be the focus of future work.

High-Barrier S_N2 Reaction. Markov models for processes with very high barrier can become numerically unstable with near degenerate eigenvalues of the transition matrix M. To test if DHAM can also be used in such high barrier examples, we carried out quantum mechanics/molecular mechanics (QM/MM) calculations[26] of the S_N2 chloride self-exchange reaction of $Cl^- + CH_3Cl \rightarrow ClCH_3 + Cl^-$ in solution (Figure 6). The simulation system consisted of the CH_3Cl and Cl^- molecules in the QM region and 2354 TIP3P water molecules in the MM region. The quantum mechanical system was coupled with the CHARMM program[27] using full electrostatic embedding.[28] We used the B3LYP[29]/6-31+G(d) density functional theory (DFT) level of theory for the QM region. We carried out 5 ps long Langevin dynamics simulations in each of the 31 umbrella windows, using a friction coefficient of 8 ps^{-1},[30] and an

DOI: 10.1021/ct500719p
J. Chem. Theory Comput. XXXX, XXX, XXX−XXX

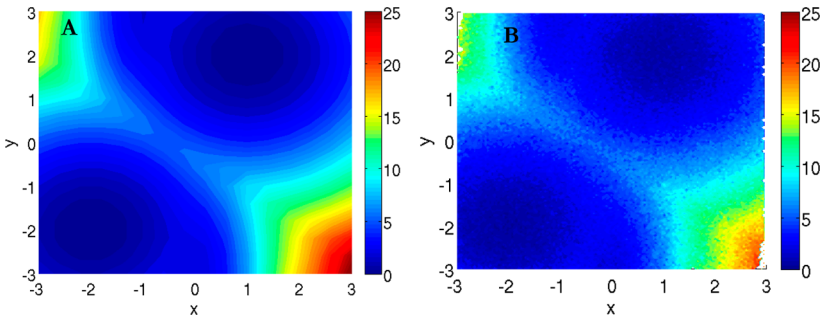

Figure 4. Original (A) and unbiased (B) 2D free energy surfaces. DHAM was used to unbias US simulations that were carried out with constraints centered on a 16 by 16 grid spanning the reaction coordinate values from −2.8 to 2.8, symmetrically for x and y.

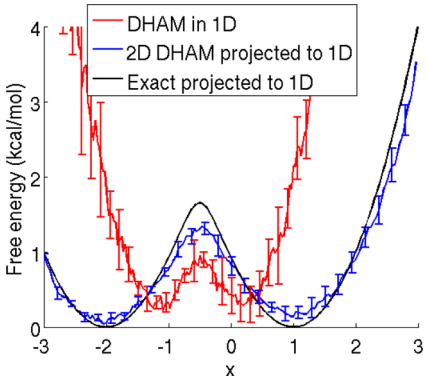

Figure 5. Effect of poor choice of reaction coordinate. Projection along the x coordinate. The projection onto x obtained using from the unbiased 2D profile obtained with DHAM (blue curve) agrees well with the exact free energy curve (black curve), whereas the 1D reconstruction of the biased simulations along x only, shows a completely different profile. The disagreement highlights the fact that the dynamics along x is non-Markovian and does not match the free energy using this poorly chosen reaction coordinate due to the presence of a hidden barrier along y, in violation of the key assumption of the DHAM model.

integration time step of 1 fs. The biasing coordinate was defined as the difference between the bond breaking and bond forming C−Cl distances, and was spaced uniformly between −3.0 and 3.0 Å. The biasing force was set to 300 kcal/mol·Å^2 in all 31 umbrella windows.

We encountered nearly degenerate eigenvalues of the transition matrix with the value of 1. In this case, DHAM is more prone to numerical errors at the transition state region. Black lines (solid and dashed) and triangles in Figure 6 show the free energies corresponding to the largest two, nearly degenerate eigenvalues of M. Indicative of mixing, the second eigenvector (Figure 6, black dashed line) does not have a node, as would be expected for a Markov matrix of a connected system. In a practical workaround, this numerical problem can be overcome by solving a subset of the set of linear equations for the equilibrium probabilities near the barrier region separately and then combining the full profile together (red lines with symbols, Figure 6). Note that here, we are not concerned with details of the reaction dynamics, for which one may want to use Hamiltonian dynamics instead of Langevin dynamics. We plan to explore dynamics in future work, including the role of inertial effects barrier crossing.[31−33] Our calculated free energy barrier of 21.5 kcal/mol agrees well with the experimental rate[34] that corresponds to a ∼24.3 kcal/mol barrier, including the cage effect.[35]

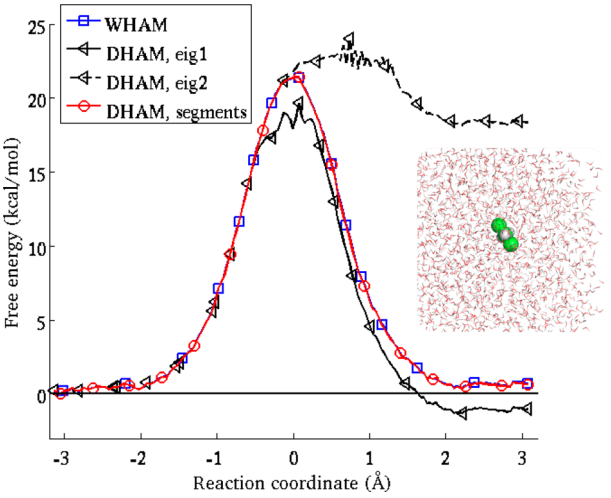

Figure 6. S_N2 reaction of CH_3Cl + Cl^-. The free energy is reconstructed using WHAM (blue lines and squares), global DHAM diagonalization of the Markov matrix (black lines and triangles), and local DHAM by determining the transition state region separately and stitching the segments together (red lines and circles). The equilibrium populations corresponding to the largest eigenvalue of the transition matrix (black solid line) mix at the transition state with the estimated equilibrium populations calculated using the second largest eigenvalue (black dashed line) due to the large barrier and sampling errors. WHAM and the DHAM segment reconstruction (red line and circles) yield practically identical results. The calculated barrier corresponds to the 24.3 kcal/mol experimental value, including the cage effect. The inset shows a snapshot of the simulation system from the transition state ensemble. The QM region is shown as spheres, and the MM water molecules are shown as licorice.

Molecular Dynamics Simulations of Na^+ in an Ion Channel. We have tested DHAM on US simulations of the passage of Na^+ ions through the transmembrane pore of the GLIC channel (Figure 7). The data was generated in the simulations of Zhu and Hummer.[23] Our method gave practically identical results as the WHAM analysis presented in the original work. This example also demonstrates that DHAM can unbias equilibrium simulations resulting in the correct converged free energy profiles even in case of inertial dynamics, such as the Langevin dynamics used here.

CONCLUSIONS

We present DHAM as an alternative to WHAM to extract free energies from umbrella sampling simulations. Both WHAM and DHAM unbias multiple biased simulations to obtain the underlying free energy profile. However, DHAM takes into

DOI: 10.1021/ct500719p
J. Chem. Theory Comput. XXXX, XXX, XXX−XXX

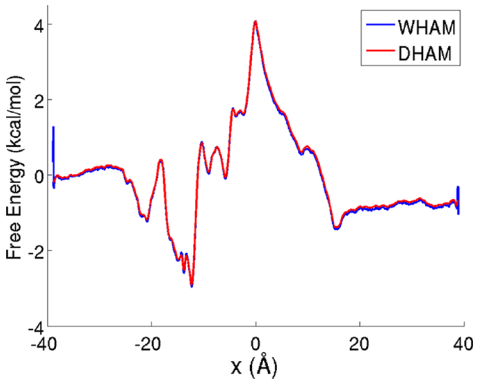

Figure 7. Umbrella sampling of a Na^+ ion in an ion channel. The free energy profile calculated with DHAM (red lines and symbols) matches perfectly the WHAM results obtained by Zhu and Hummer[23] (blue line). Note that no constraint was imposed to match the free energy profiles on opposite sides of the membrane.

account the dynamics and time sequence, and does not require that equilibrium is reached in each US window along the reaction coordinate. DHAM is based on discretizing the biased reaction coordinates, using these discrete bins as microstates, and determining a Markov matrix of transition probabilities between the bins using a maximum-likelihood approach.

We showed that WHAM is prone to significant errors when used in combination with weak biasing potentials. Such errors arise even if only a few biased simulations do not fully sample the corresponding equilibrium probabilities along the whole reaction coordinate. By contrast, the local transition probabilities in DHAM can be considered well-converged even if the global equilibrium populations are not fully sampled. Correspondingly, we found that in such cases the DHAM free energies converge faster as a function of simulation length than those of WHAM, with DHAM estimates being more accurate by overcoming the significant error associated with weak bias in the umbrella sampling.

We obtained a simple noniterative approximation for the underlying transition matrix in the limit of short lagtimes. Throughout the paper we used this approximation to calculate free energies. We also present the formulation and implementation for unbiasing uncorrelated data with long lagtimes, and show that in the limit of fully uncorrelated data we recover the WHAM solution.

We compared WHAM and DHAM by analyzing MC umbrella sampling simulations using an asymmetrical double well model potential. When strong biasing forces are used, the two methods perform similarly well, and have comparable statistical errors. However, we show that WHAM has a significant error when weak biasing potentials are used. By contrast, DHAM provides accurate estimates of the free energy profile if they are consistent with the underlying dynamics. If inadequate low-dimensional coordinates are used, however, we find that the DHAM estimates differ from the free energy calculated as the projection of the appropriate high-dimensional problem. A comparison of DHAM and WHAM results can thus be used as a test for the dynamic relevance of the chosen coordinate. In addition, DHAM can also be used to obtain the underlying free energy profile from unbiased downhill simulations. We demonstrate that DHAM can be used to calculate the free energy profile for the high-barrier QM/MM US simulations of the self-exchange S_N2 reaction of $CH_3Cl + Cl^-$ in explicit water. In this case, however, DHAM is numerically more prone to errors due to the degeneracy of the transition probability matrix, and a segment based approach is introduced for calculating the free energy profile. We demonstrate that DHAM provides converged free energies in this example as compared to WHAM. Our method was also successfully applied to calculate the free energy profile of a Na^+ ion passing through the transmembrane pore of the GLIC channel from US MD simulations. In this case, DHAM provides identical free energy estimates compared to WHAM.

In practical applications, DHAM complements and extends WHAM, providing an indicator of possible problems in WHAM calculations. In particular, deviations between WHAM and DHAM free energies suggest that dynamic corrections are important. DHAM should help identify the resulting problems even in cases where the Markov state model may not be fully adequate, such as cases where even the local dynamics is non-Markovian. To pinpoint the origin of discrepancies between WHAM and DHAM, one can compare the local relaxation times, as calculated from the global Markov matrix, to the simulation times in each window, and to the relaxation times calculated directly by integrating the position autocorrelation functions in each window.

By going beyond the calculation of free energies, our approach of combining trajectories with different biasing potentials may also prove useful in the construction of global Markov state models from locally biased simulations. DHAM thus produces not only free energies but also kinetic information, which we here used to assess whether simulations are sufficiently long to achieve equilibrium sampling. In the future, we plan to use DHAM also to estimate rates directly from umbrella sampling simulations.

APPENDIX A

WHAM Solution for Non-Overlapping Data

In the following, we illustrate the error in the WHAM free energy for systems that are not sampling all umbrella windows. To keep the problem analytically tractable, we use a simple model with only two possible configurations, at points x_1 and x_2, separated by an insurmountable barrier. This model mimics situations in which a molecular system has two states, such as "folded" and "unfolded", that exchange only on time scales much longer than the simulations. For our two-state model, the simulation data consist of two sets of trivial trajectories, in one of the windows N_1 steps sampling x_1, and in the other window N_2 steps sampling x_2. There is thus no overlap between the two simulations. Nevertheless, WHAM provides an estimate for the free energy difference between the two states. The WHAM expressions for the relative equilibrium populations p_1 and p_2 in the bins 1 and 2 containing x_1 and x_2 are

$$p_1 = \frac{N_1}{N_1\, e^{-\beta V_1(x_1)} + N_2 f_2\, e^{-\beta V_2(x_1)}} \tag{A1}$$

$$p_2 = \frac{N_2}{N_1\, e^{-\beta V_1(x_2)} + N_2 f_2\, e^{-\beta V_2(x_2)}} \tag{A2}$$

We introduce $c_{ij} = e^{-\beta V_i(x_j)}$ with $c_{11} = c_{22} = 1$. For most biasing potentials, we have $c_{12}, c_{21} \ll 1$ and thus

$$e^{-\beta \Delta G} = \frac{p_2}{p_1} = \frac{N_2}{N_1} \frac{N_1 + N_2 f_2 c_{21}}{N_1 c_{12} + N_2 f_2} \approx \frac{1}{f_2} \tag{A3}$$

DOI: 10.1021/ct500719p
J. Chem. Theory Comput. XXXX, XXX, XXX−XXX

Using the binless formulation for the WHAM equations[5−7] we can also determine f_2 exactly:

$$\frac{1}{f_2} = \frac{N_1 c_{21}}{N_1 c_{11} + N_2 f_2 c_{21}} + \frac{N_2 c_{22}}{N_1 c_{12} + N_2 f_2 c_{22}} \tag{A4}$$

This equation can be simplified to

$$0 = f_2^2 + \frac{N_1 - N_2}{N_2} c_{12} f_2 - \frac{N_1}{N_2}\frac{c_{12}}{c_{21}} \tag{A5}$$

For typical simulation settings this leads to $f_2 \approx ((N_1/N_2)(c_{12}/c_{21})^{1/2}$ and $e^{-\beta\Delta G} \approx ((N_2/N_1)(c_{21}/c_{12}))^{1/2}$.

Considering an umbrella sampling simulation with two windows centered at x_1 and x_2, using a harmonic bias with spring constants K_1 and K_2, respectively, for each window, WHAM thus gives the following estimate for the free energy difference:

$$\frac{p_2}{p_1} = e^{-\Delta G/k_B T} \approx \sqrt{\frac{N_2}{N_1}}\, e^{-(x_2 - x_1)^2 (K_2 - K_1)/4 k_B T} \tag{A6}$$

$$\Delta G \approx (x_2 - x_1)^2 (K_2 - K_1)/4 + k_B T/2 \ln \frac{N_1}{N_2} \tag{A7}$$

This WHAM estimate ΔG of the free energy difference is entirely artificial, since no equilibrium has been achieved due to the insurmountable barrier. The least significant error is made when $K_1 = K_2$ and $N_1 = N_2$, in which case $\Delta G = 0$.

APPENDIX B

Full Maximum Likelihood Solution

To find the maximum of the log-likelihood L, subject to the normalization constraints, we substitute the explicit expression for M_{ji} in eq 12 into eq 10 for $f_i^{(k)}$. This results in $Nbin$ sets of $Msim$ nonlinear equations in the $f_i^{(k)}$ $(k = 1, ..., Msim)$ and μ_i:

$$f_i^{(k)} = \left(\sum_{j=1}^{Nbin} c_{ji}^{(k)} \frac{\sum_{m=1}^{Msim} T_{ji}^{(m)}}{\mu_i + \sum_{m=1}^{Msim} n_i^{(m)} f_i^{(m)} c_{ji}^{(m)}} \right)^{-1} \tag{B1}$$

By setting also the derivative of L with respect to μ_i to zero, we obtain the normalization conditions for each i:

$$\sum_{j=1}^{N_{bin}} M_{ji} = \sum_{j=1}^{N_{bin}} \frac{\sum_{k=1}^{Msim} T_{ji}^{(k)}}{\mu_i + \sum_{k=1}^{M_{sim}} n_i^{(k)} f_i^{(k)} c_{ji}^{(k)}} = 1 \tag{B2}$$

In eqs B1 and B2, we have thus obtained closed sets of $(Msim + 1)$ coupled nonlinear equations for each i in the $(Msim + 1)$ parameters $f_i^{(k)}$ $(k = 1, ..., Msim)$ and μ_i. The different sets of nonlinear equations are uncoupled and can thus be solved separately for each bin index $i = 1, 2, ..., N_{bin}$.

To solve the $(Msim + 1)$ coupled nonlinear eqs B1 and B2 for each i, one can use a variety of numerical methods, from multidimensional Newton−Raphson type solutions to direct iteration. We found that a direct iteration for the $f_i^{(k)}$ by evaluating the right-hand-side of eq B1 combined with a Newton-Raphson solution of the 1D polynomial eq B2 for μ_i works well, starting with $f_i^{(k)} = 1$ and $\mu_i = 0$, or with the initial guess of $f_i^{(k)}$ calculated from the explicit analytic approximation eq 22 via eqs 21 and 10. The iteration of the $f_i^{(k)}$ can be accelerated or dampened by mixing the new and old estimates. With this iterative procedure, solutions can be found for all i and weight parameters w between 1/2 and 1. The corresponding log-likelihood can then be calculated from eq 7, where the terms involving the Lagrange multipliers vanish exactly since the solutions satisfy all constraints. The family of solutions for different w then gives an indication of the sensitivity to the choice of the coefficient matrix. The optimal w can be chosen according to the maximum of the likelihood. Indeed, we could also have maximized with respect to w directly, though that would couple the sets of equations for the different bins i.

Interestingly, in test cases we considered, the full likelihood optimization performed significantly worse than the approximate DHAM method of the main text, even in cases where values of $w > {}^1/_2$ would seem appropriate. Apparently, full optimization can produce models that describe the overall dynamics better (as indicated by the higher likelihood values), but not necessarily the underlying free energy surface. This is possibly a result of violations of detailed balance, which is enforced at least partially in the construction of the approximate DHAM solution eq 19. In general, we also cannot expect that a single w value would be appropriate for all regions of the reaction coordinate space, and for all the simulations involved. For this reason, we here advocate the simple, robust, and non-iterative DHAM method described in the main text.

In conclusion of this Appendix, we note that detailed balance has not been enforced in the construction of the transition matrix M_{ji}. Since the dynamic model is only approximate, we consider this here a minor issue. In fact, a transition matrix that does not obey detailed balance can potentially highlight convergence problems. To assess the deviations from detailed balance, we can for instance calculate the ratio of the unbalanced and total fluxes between the bins:

$$\eta = \frac{\sum_{i<j}^{N_{bin}} |M_{ij} p_j - M_{ji} p_i|}{\sum_{i<j}^{N_{bin}} M_{ij} p_j + M_{ji} p_i} \tag{B3}$$

One could also explicitly enforce detailed balance in the construction of the transition matrices following Sriraman et al.,[16] who used the normalized equilibrium probabilities and the transition rates between states $i > j$ to construct the transition rates between states $j > i$. Alternatively, an appropriate Bayesian prior can also be imposed,[36,37] or detailed balance can be enforced through constraints on all cycles, $M_{jk} M_{ki} M_{ij} = M_{kj} M_{ik} M_{ji}$ for all $i < j < k$ and $f_i^{(k)} = f_j^{(k)}$ for all $i < j$. However, in either case the simplicity of the final expressions derived here for the transition matrix would be lost.

AUTHOR INFORMATION

Corresponding Author

*E-mail: edina.rosta@kcl.ac.uk.

Notes

The authors declare no competing financial interest.

ACKNOWLEDGMENTS

We thank Dr. Attila Szabo and Prof. Frank Noé for their comments and suggestions, and Prof. Fangqiang Zhu for kindly providing us his simulation data. We acknowledge the use of the National Institutes of Health (NIH) Biowulf cluster and the EPSRC U.K. National Service for Computational Chemistry Software (NSCCS) at Imperial College London. G.H. was supported by the Max Planck Society.

REFERENCES

(1) Torrie, G. M.; Valleau, J. P. *J. Comput. Phys.* **1977**, *23*, 187.

DOI: 10.1021/ct500719p
J. Chem. Theory Comput. XXXX, XXX, XXX−XXX

(2) Kumar, S.; Rosenberg, J. M.; Bouzida, D.; Swendsen, R. H.; Kollman, P. A. *J. Comput. Chem.* **1992**, *13*, 1011.
(3) Ferrenberg, A. M.; Swendsen, R. H. *Phys. Rev. Lett.* **1989**, *63*, 1195.
(4) Bennett, C. *J. Comput. Phys.* **1976**, *22*, 245.
(5) Shirts, M.; Chodera, J. *J. Chem. Phys.* **2008**, *129*, 124105.
(6) Tan, Z.; Gallicchio, E.; Lapelosa, M.; Levy, R. M. *J. Chem. Phys.* **2012**, *136*, 144102.
(7) Rosta, E.; Nowotny, M.; Yang, W.; Hummer, G. *J. Am. Chem. Soc.* **2011**, *133*, 8934.
(8) Wu, H.; Noé, F. *Multiscale Model. Simul.* **2014**, *12*, 25.
(9) Sakuraba, S.; Kitao, A. *J. Comput. Chem.* **2009**, *30*, 1850.
(10) Noé, F.; Fischer, S. *Curr. Opin. Struct. Biol.* **2008**, *18*, 154.
(11) Noé, F.; Horenko, I.; Schütte, C.; Smith, J. C. *J. Chem. Phys.* **2007**, *126*, 155102.
(12) Chodera, J. D.; Noé, F. *Curr. Opin. Struct. Biol.* **2014**, *25*, 135.
(13) Pande, V. S.; Beauchamp, K.; Bowman, G. R. *Methods* **2010**, *52*, 99.
(14) Hummer, G.; Kevrekidis, I. G. *J. Chem. Phys.* **2003**, *118*, 10762.
(15) Adib, A. *J. Chem. Phys.* **2005**, *124*, 144111.
(16) Sriraman, S.; Kevrekidis, I. G.; Hummer, G. *J. Phys. Chem. B* **2005**, *109*, 6479.
(17) Mey, A. S.; Wu, H.; Noé, F. *Phys. Rev. X* **2014**, *4*, 041018.
(18) Bicout, D. J.; Szabo, A. *J. Chem. Phys.* **1998**, *109*, 2325.
(19) Gallicchio, E.; Andrec, M.; Felts, A. K.; Levy, R. M. *J. Phys. Chem. B* **2005**, *109*, 6722.
(20) Hummer, G. *New J. Phys.* 2005, *7*, 34.
(21) Rosta, E.; Nowotny, M.; Yang, W.; Hummer, G. *J. Am. Chem. Soc.* **2011**, *133*, 8934.
(22) Buchete, N.-V.; Hummer, G. *J. Phys. Chem. B* **2008**, *112*, 6057.
(23) Zhu, F.; Hummer, G. *J. Comput. Chem.* **2012**, *33*, 453.
(24) Zhang, Q.; Brujić, J.; Vanden-Eijnden, E. *J. Stat. Phys.* **2011**, *144*, 344.
(25) Rosta, E.; Woodcock, H. L.; Brooks, B. R.; Hummer, G. *J. Comput. Chem.* **2009**, *30*, 1634.
(26) Warshel, A.; Levitt, M. *J. Mol. Biol.* **1976**, *103*, 227.
(27) Brooks, B. R.; Bruccoleri, R. E.; Olafson, B. D.; States, D. J.; Swaminathan, S.; Karplus, M. *J. Comput. Chem.* **1983**, *4*, 187.
(28) Woodcock, H. L., 3rd; Hodoscek, M.; Gilbert, A. T.; Gill, P. M.; Schaefer, H. F., 3rd; Brooks, B. R. *J. Comput. Chem.* **2007**, *28*, 1485.
(29) Becke, A. *J. Chem. Phys.* **1993**, *98*, 5648.
(30) Pastor, R. W.; Brooks, B. R.; Szabo, A. *Mol. Phys.* **1988**, *65*, 1409.
(31) Castillo, R.; Roca, M.; Soriano, A.; Moliner, V.; Tuñón, I. *J. Phys. Chem. B* **2007**, *112*, 529.
(32) Grote, R. F.; Hynes, J. T. *J. Chem. Phys.* **1980**, *73*, 2715.
(33) Peters, B. *Chem. Phys. Lett.* **2012**, *554*, 248.
(34) Albery, W. J.; Kreevoy, M. M.; Gold, V.; Bethell, D. *Adv. Phys. Org. Chem.* **1978**, *16*, 87.
(35) Yang, S.-Y.; Fleurat-Lessard, P.; Hristov, I.; Ziegler, T. *J. Phys. Chem. A* **2004**, *108*, 9461.
(36) Diaconis, P.; Rolles, S. W. W. *Ann. Statist.* **2006**, *34*, 1270.
(37) Bacallado, S.; Chodera, J. D.; Pande, V. *J. Chem. Phys.* **2009**, *131*, 045106.

DOI: 10.1021/ct500719p
J. Chem. Theory Comput. XXXX, XXX, XXX−XXX